Appl. Phys. B (2013) 110:367–373
DOI 10.1007/s00340-012-5263-7

Applied Physics B
Lasers and Optics

Domain inversion in $LiNbO_3$ and Zn-doped $LiNbO_3$ crystals by the electron-beam irradiation of the nonpolar *Y*-surface

L. S. Kokhanchik · T. R. Volk

Received: 25 April 2012 / Revised: 5 September 2012 / Published online: 21 November 2012
© Springer-Verlag Berlin Heidelberg 2012

Abstract Individual domains and domain gratings were fabricated on nonpolar *Y*-cuts of $LiNbO_3$ and $LiNbO_3$-Zn crystals by electron beam irradiation. The domains which nucleated in the irradiation points are frontally growing along the direction $+Z$ within a thin (of about several microns) surface layer. The regularities of this motion are discussed in the framework of the approach to formation of space-charge fields under e-beam charging of insulators. The obtained dependency of the domain length on the exposure time permits us to propose the viscous-friction mechanism for the observed frontal domain growth. The velocity of the frontal growth in $LiNbO_3$-Zn is higher than in $LiNbO_3$ obviously due to a decreased number of pinning centers at the Nb-antisites. In $LiNbO_3$-4 %Zn crystals planar domain gratings were fabricated by means of point-to-point irradiations along the *X*- and *Z*-directions with specified distances between the irradiation points. It is shown that the domain gratings are generated by a total field of point charges $\vec{E} = \sum_{i=1}^{n} \vec{E}_i$, where E_i is the space-charge field induced in any irradiation point, and n is the number of points. Some preliminary estimates indicate that the frontal growth of domains under e-beam irradiation occurs at fields $E < E_c$.

L. S. Kokhanchik
Institute of Microelectronics Technology and High Purity Materials of the Russian Academy of Sciences, Chernogolovka, 142432 Moscow, Russia

T. R. Volk (✉)
Institute of Crystallography Russian Academy of Sciences, Leninski prospect 59, 119333 Moscow, Russia
e-mail: volk@crys.ras.ru

1 Introduction

Ferroelectric domain structures with specified design are of particular interest for optical frequency conversion. The most prominent material for these aims is lithium niobate due to the large quadratic nonlinear susceptibility and a high stability of the regular domain structures (RDS) fabricated by various methods. One of the topical problems is the frequency conversion in optical waveguides based on $LiNbO_3$. Certain future applications, such as nonlinear photonic crystals or optical schemes with semiconductor laser diodes require RDS periods of about 2–4 μm or even of submicron range. The preparation of so small-scaled RDS in $LiNbO_3$ with the aid of the field method (by means of applying high voltages to a patterned electrode deposited on the polar surface) meets certain technological and fundamental problems. Additionally, the field method does not allow to produce RDS on the nonpolar (*X*- or *Y*-) surfaces which sometimes are more preferable for producing optical waveguides than the polar *Z*-cut. The most promising methods for the creation of microdomain arrays use local poling with the help of electron-beams in a scanning electron microscope (SEM) or applying dc-voltages to an AFM tip (see [1]). There is a number of publications devoted to the fabrication of domains and RDS on polar cuts of $LiNbO_3$ crystals using the SEM method, e.g. [2–7] (more detailed bibliography can be found, e.g. in [1]). Recently, one of the present authors (L. K.) succeeded in recording domains and RDS on nonpolar (*X*- and *Y*-) cuts of $LiTaO_3$ crystals by means of e-beam irradiation [8]. Later on, similar results were obtained in $LiNbO_3$ [9]. Additionally, domain gratings were fabricated by this method in Ti-indiffused planar waveguides on *Y*-cuts of $LiNbO_3$ crystals. With these gratings QPM waveguide SHG from 1053 radiation was observed [9].

This paper presents electron-beam recording of domains and domain gratings on *Y*-cut $LiNbO_3$-Zn crystals. For comparison, e-beam domain recording was performed under similar exposure conditions in the nominally pure $LiNbO_3$ crystals. The choice of $LiNbO_3$:Zn is owing to the well-known effects of the Zn impurity on the properties of $LiNbO_3$. Firstly, Zn-doping reduces drastically the optical damage in $LiNbO_3$ [1], and, secondly, Zn-indiffusion provides the optical waveguide effect [10]. Therefore, the results obtained are useful for projected e-beam recording of RDS in optical-damage resistant Zn-$LiNbO_3$ optical waveguides. Moreover, we attempt, for the first time to our knowledge, to discuss qualitatively the domain formation under e-beam irradiation in the framework of the current approach to the formation of space-charge fields in insulators under e-beam charging.

2 Crystals and experimental procedures

$LiNbO_3$ crystals of congruent composition (designated below as CLN) and $LiNbO_3$-Zn crystals were grown by the Czochralsky method. As known, a drastic decrease of the optical damage occurs at a "threshold" Zn concentration of about 6–7 at.% in the crystal [1]. The crystals under study were doped with 4 and 7.5 at.% Zn (designated below as LN-4Zn and LN-7.5Zn, respectively), thus below and above the photorefractive threshold. The samples were optically polished *Y*-cut plates of 1 mm thickness. Domain recording was performed in a JSM-840A SEM by an electron beam incident normally onto the *Y*-surface. The opposite side of the crystals was covered by a grounded Al layer. The experiments were carried out at a beam energy of $U_0 = 25$ keV, and currents of $I = 0.1$ or 1 nA. The apparatus was equipped with the NanoMaker program which allowed us to control both the electron beam when scanning over the surface and the irradiation dose $D = It_{irr}/S_{irr}$, where I is the current, t_{irr} is the exposure time, and S_{irr} is the area of local irradiation. A set of individual domains was produced via local irradiations of the *Y*-surface by discrete displacements of the beam along the *Z*- or *X*-direction. The recording was performed for three areas of the local irradiation $S_{irr} = 0.5$, 1 and 4 μm^2; the exposure time was varied in the range from 30 to 1040 ms. In Sect. 3.2 we describe in detail the fabrication of the domain gratings by this technique.

The produced domains and domain gratings were visualized by selective chemical etching of the samples in a boiling solution of the $HF + 2HNO_3$ acids during 60 s. As known [11, 12], the negative *Y*-surface of $LiNbO_3$ chemically etches much faster than the positive one. Thus, selective etching reveals the domains recorded on the $-Y$ and $+Y$ surfaces as long triangular hillocks and grooves, respectively. All the results presented below were obtained on the $-Y$ surfaces. The height of the etched hillocks was evaluated using a Zeiss Axioplan 2 interference optical microscope [9]. These results were supported by several AFM measurements.

3 Experimental results and discussion

3.1 The formation of individual (single) domains

The data of [8, 9] have revealed the following scenario of the domain evolution: Local irradiation of the *Y*-faces of $LiNbO_3$ and $LiTaO_3$ crystals leads to formation of a single domain which is growing from the irradiated spot along the polar axis *Z* parallel to the sample surface. Domain growth always occurs in the $+Z$ direction. The results obtained in the present work are consistent with this scenario. Figure 1a and b exemplifies micrographs of etched

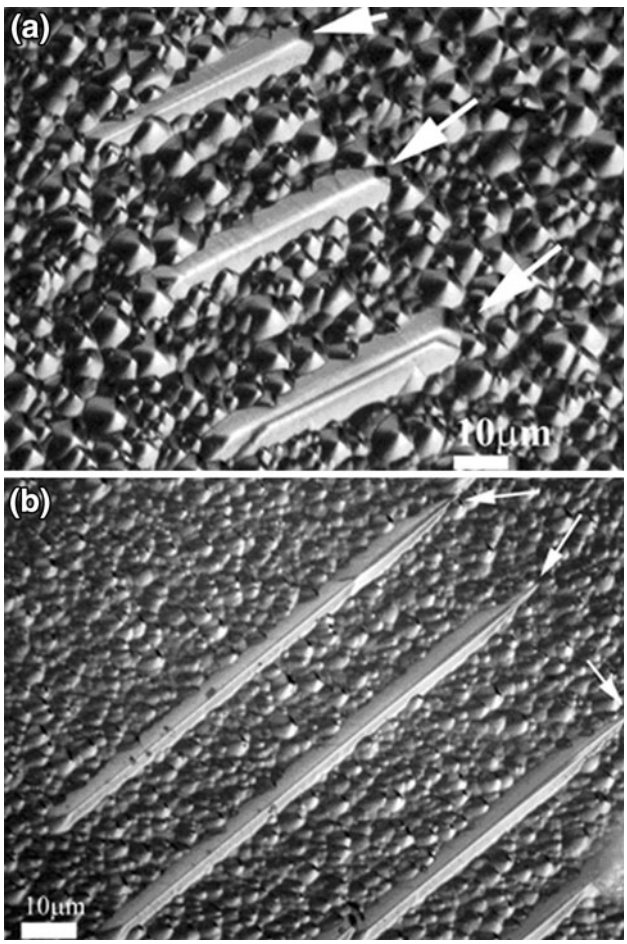

Fig. 1 The micrographs of the etched domains fabricated on negative *Y*-surfaces in $LiNbO_3$ (**a**) and $LiNbO_3$-4 %Zn (**b**); the *arrows* show the irradiation points. The experimental conditions were $U_0 = 25$ keV, $I = 0.1$ nA, $S_{irr} = 1$ μm^2, $t_{irr} = 200$ ms. The domains are oriented along the *Z*-axis

individual domains produced by local irradiation of the negative *Y*-cuts in CLN and LN-4Zn crystals ($I = 0.1$ nA, $S = 0.5$ μm^2, $t_{irr} = 200$ ms). As seen, in LN-4Zn the domains are narrowed towards the irradiation area, whereas in CLN a gradual domain narrowing seems to occur at the final growth stage.

The characteristics of domain recording in LN-4Zn and CLN are qualitatively similar and discussed together. The process in the optical-damage resistant LN-7.5Zn is qualitatively different and will be described separately.

To record domains in LN-4Zn and CLN crystals, we used a beam voltage and current of $U_0 = 25$ kV, $I = 0.1$ nA, respectively. For these exposure conditions, the minimum irradiation times required for revealing domains are $t_{irr} \approx 40$–50 ms which correspond to an implanted charge of $Q \approx 4$–5 pC, i.e. to irradiation doses of $D \approx Q/S_{irr} = (1$–$10)$ C/m^2 for the used range of local irradiation areas.

Figure 2 and the inset depict the exposure dependencies of l_d on t_{irr}. As seen, the domain length l_d grows with t_{irr} with no trend towards saturation. The experimental points in Fig. 2 were obtained at $S_{irr} = 4$ μm^2 up to longest exposure times $t_{irr} = 1400$ ms. In the inset we show the data obtained at varied irradiation areas $S_{irr} = 0.5$, 1 and 4 μm^2. The solid lines show the linear approximation of the experimental data. In the inset the solid lines present the linear approximation over all experimental points at varied S_{irr}. The plots $l_d(t_{irr})$ in both crystals are well approximated by two linear functions $y = a + bx$ with a salient point at about $t_{irr} \approx 200$–300 ms. Below the salient point $b = 0.22$ and 0.33 in CLN and LN-4Zn, respectively; above the salient point $b = 0.1$ and 0.14 in CLN and LN-4Zn, respectively. So, in the whole exposure range the achieved domain lengths in LN-4Zn are by a factor of about 1.5 larger than in CLN at equal exposure conditions. As can be seen from the inset, the dependencies $l_d(t_{irr})$ in a certain crystal obtained with varied irradiation areas are well fitted by a single linear function (solid lines in the inset), i.e. $l_d(t_{irr})$ is practically not affected by S_{irr}. In other words, at a constant beam current the length of a growing domain is governed by the irradiation time rather than by the implanted charge $Q = D\,S_{irr}$ as could be expected.

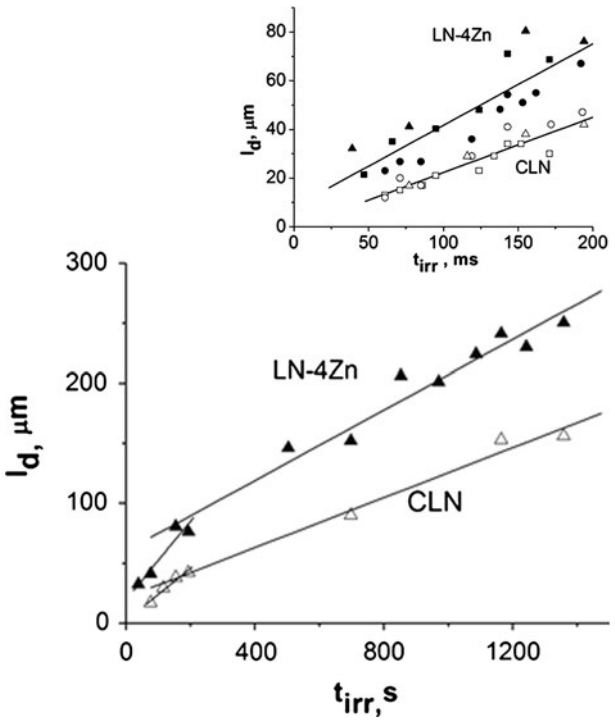

Fig. 2 The dependencies of the domain length on the irradiation time in $LiNbO_3$ and $LiNbO_3$-4 %Zn crystals at the local irradiation area $S = 4$ μm^2: The *inset* shows the data obtained for varied irradiation areas in the range of short irradiation times; the squares, circles and triangles correspond to $S = 0.5$, 1 and 4 μm^2, respectively, the open and solid symbols correspond to CLN and LN-4Zn, respectively. The *solid lines* represent the fit of the experimental points by the linear functions $y = a + bx$; the values are given in the text

The domain width along the *X*-axis is within 5–6 μm and almost independent of S_{irr} and t_{irr}. The height of the domain hillocks, corresponding to the domain thickness along the *Y*-direction is of about 4–5 μm both in CLN and LN-4Zn. So, in accordance with the previous results in $LiNbO_3$ [9], the domain evolution in this peculiar situation occurs predominantly by the frontal (transit) growth along the polar direction in a thin surface layer, whereas the lateral domain-wall motion is negligible.

In order to discuss these results in terms of ferroelectric switching, let us describe very briefly the formation of space-charge fields in a crystal irradiated by an electron beam. A detailed review of this situation is beyond the aim of the present work, therefore our considerations are based on recent reviews and original papers [13–16]. When the surface of an insulator crystal is bombarded by an electron beam using the spot mode of an SEM, the region of the space charge Q_{sc} formed by the trapped electrons can be represented as a truncated sphere. Its radius is determined by the penetration depth R_e of the primary electrons, which in turn depends on the electron energy U_0 and the properties of the crystal. The equilibrium value of R_e can be described by a generalized power function.

$$R_e = AU_0^k/\rho \tag{1}$$

where ρ is the crystal density, the exponent $k = 1.7$ [17, 18] and 2 [19], and a dimensionless coefficient $A = 45.7$ [17], 78.9 [18] and 25 [19]. Taking into account $\rho = 4.65$ and 4.73 g/cm^3 for CLN and LN-4Zn, respectively, the evaluation for $U_0 = 25$ keV gives an average $R_e = (2$—$4)$ μm. This estimate is very close to the value calculated in [4]. The space-charge field E_{sc} may be approximated by the field of a point charge located at a depth

$a = R_e/2$ beneath the surface. For a semi-infinite insulator a simplified expression for the distribution of the field component directed along the polar Z axis can be expressed as:

$$E_z(r) = \frac{Q_{sc}}{4\pi\sqrt{\varepsilon_z\varepsilon_x}\varepsilon_0}\left(\frac{r}{\left[r^2 + \left(2a/\sqrt{\frac{\varepsilon_z}{\varepsilon_x}}\right)^2\right]^{3/2}} + \frac{1}{r^2}\right) \quad (2)$$

where Q_{sc} is the space charge, r is the distance from the irradiation area along the polar direction, and ε_z and $\varepsilon_x = \varepsilon_y$ are the dielectric permittivities. The kinetics of Q_{sc} is a complicated process depending on a whole set of the interrelated processes, such as the trapping and backscattering of the primary electrons, the emission of the secondary electrons, the radiation-induced increasing of the conductivity, etc. The available models of the electron-beam charging of insulators lead to the following generalized expression for the kinetics of the space-charge [13, 15, 16] for given U_0 and I

$$Q_{sc}(t) = Q_{sc}^{sat}[1 - \exp(-t/\tau_{eff})] \quad (3)$$

The effective time constant τ_{eff} describes the time required for trapping and detrapping process to reach equilibrium. This is an empirical parameter dictated both by the irradiation conditions and properties of the irradiated material, particularly by the radiation-induced conductivity. All other conditions being equal, $\tau_{eff} \approx 1/U_0$. The complexity of the problem rules out the possibility of any reliable calculations of τ_{eff}. Regardless of the models used, a wealth of experimental data cited, e.g. in [13, 15] indicates that for the beam energies in the range (10–30) keV the time τ_{eff} in the high-resistance insulators to which $LiNbO_3$ belongs ($\rho = 10^{14}$–10^{16} Ohm m), is as large as hundreds of milliseconds and even larger.

On this basis, one may suggest that the salient point observed in the plots $l_d(t_{irr})$ at certain $t_{irr}' = 200$–300 ms (Fig. 2) corresponds to the occurrence of the dynamic charge equilibrium. This means that at $t_{irr} > t_{irr}' \approx \tau_{eff}$ the charge Q_{sc} reaches a saturation quasi-steady value and for further increasing of t_{irr} the field $E_{sc} \approx$ const. The validity of this assumption is supported by the shape of $l_d(t_{irr})$ plots. Actually, at $t_{irr} > t_{irr}'$ the domain length is a linear function of t_{irr} (Fig. 2), i.e. the average velocity of the frontal (transit) domain motion $v_{tr} = dl_d/dt =$ const. Since the velocity of the domain motion regardless of the switching mechanism depends on the field [20, 21], the constancy of v_{tr} with increasing t_{irr} argues unambiguously of a constant field.

We remind again that in our case the domain motion occurs dominantly by frontal growth. According to the classical model of the ferroelectric switching [20, 21], frontal domain growth through the bulk of the crystal follows a law analogous to a viscous friction,

$$v_{tr} = kE \sim \mu E \quad (4)$$

where E is the external field and μ is the domain-wall mobility. In the law (4), the domain length under a constant field is proportional to the time of the field applying, $l_d = v_{tr}\, t$. Therefore, the linear plots $l_d(t_{irr})$ (Fig. 2) indicate that the observed motion of a planar domain within a thin layer occurs via this mechanism (4).

Let us make some quantitative estimates of the fields controlling the domain growth. The domain motion ceases when the field in the vicinity of the "head" of a growing domain falls down below certain E_{fin}. The value of E_{fin} is determined by the spatial distribution $E(r)$ given by Eq. (2). We estimated the fields E_{fin} by means of substituting into Eq. (2) the values $r = l_d$ taken from the plots $l_d(t_{irr})$ of Fig. 2 ($\varepsilon_z = 29$; $\varepsilon_y = \varepsilon_x = 84$, $a = 3$ μm, see above). Figure 3 presents the dependencies $E_{fin}(t_{irr})$ calculated for $t_{irr} > t_{irr}'$. As seen, within this range of the exposure times the field $E_{fin} \approx$ const. This result is expected assuming E_{sc} not to change for $t_{irr} > t_{irr}'$. The averaged values of E_{fin} for LN and LN-4Zn are 4.3 10^6 and 2.8 10^6 V/m, respectively.

To verify these estimations, we evaluated the fields by an alternative method proposed in [3]. In order to characterize the electron-beam recording of domains on the Z-cuts of $LiNbO_3$, the authors of [3] evaluated the fields on the basis of the exposure doses D. As mentioned above, in our case the domains appear at $D \approx$ (1–10) C/m^2. The calculations taking into account the total electron emission yield $\sigma \approx 0.5$–0.6 [22] give for these doses the field $E_d \approx 10^8$ V/m in the immediate vicinity of the irradiation area. For these D corresponding to $t_{irr} \approx 40$–50 ms, the domain lengths are $l_d = 20$–25 μm (Fig. 2). As the field decreases approximately by $\approx 1/r^2$, so 20–25 μm away from the irradiation area the field E_d decreases to $E \approx 10^6$ V/m. This value is in a good agreement with E_{fin} (Fig. 3) and supports the validity of the field estimates based on $l_d(t_{irr})$

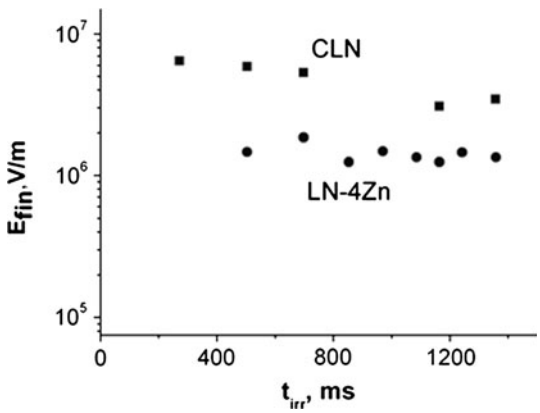

Fig. 3 The exposure dependencies of the field E_{fin} corresponding to the completion of the frontal domain growth at a given irradiation time (for details see text). The *squares and circles* correspond to $LiNbO_3$ and $LiNbO_3$-4 %Zn, respectively

It is reasonable to correlate E_{fin}, which governs the completion of the frontal domain growth, to the macroscopic coercive fields E_c in the same crystals. As known, in CLN the threshold field of the polarization reversal is $E_c = 2.2\ 10^7$ V/m [1]. Doping $LiNbO_3$ with the optical-damage resistant impurities is accompanied by a gradual decrease of E_c with increasing concentrations [1]. The strong decrease of E_c in $LiNbO_3$-Zn at [Zn] > 5 % [23] in combination with the detailed measurements of E_c in $LiNbO_3$-Mg [24], permit us to suggest an $E_c \geq 1.5\ 10^7$ V/m for LN-4Zn. So, the fields E_{fin} corresponding to the stop of the frontal domain growth in CLN and LN-4Zn ($4.8\ 10^6$ and $1.4\ 10^6$ V/m, respectively) are noticeably lower than E_c in these crystals. In other words, the domains continue their frontal motion up to the fields $E < E_c$ (assuming the classical definition of E_c).

Although we are aware that our field estimates are very approximate, nonetheless, a couple of data in the related publications support this conclusion. Extended surface domains were fabricated in $LiNbO_3$ by applying high voltages to a needle-like electrode contacting the *Y*-face [25–27]. Our estimates of the results reported in [25–27] have found that frontal domain growth occurred under $E << E_c$. The frontal domain motion under $E << E_c$ was detected when recording domains in a high-voltage AFM (HVAFM) on the $LiNbO_3$ polar cuts [28, 29]. The common feature in all these cases is a high field strength in the vicinity of the point of the domain nucleation, namely, $E_d \approx 10^8$ V/m in our case and in [25–27] and $E \approx 10^9$ V/m [28, 29]. According to the model proposed for ferroelectric switching using HVAFM [29], the energy δ of the domain nucleation under conditions of strong local fields is very low. As a result, the rate of the switching process is governed by the domain-wall motion rather than by the domain nucleation in contrast to the classical model [20, 21]. The domain motion in fields $E < E_c$ deduced from the $l_d(t_{irr})$ curves in our case, indicates that the switching mechanism under electron-beam irradiation differs qualitatively from the usual scenario.

The velocity of the frontal domain growth in LN-4Zn is noticeably higher than in CLN (Fig. 2). Similar increase of the velocity of the lateral domain-wall motion was observed in $LiNbO_3$-5.5 %Mg as compared with CLN [30]. According to the current model of the defect structure of $LiNbO_3$ [1], the effects of optical-damage resistant impurities on the properties of $LiNbO_3$ are qualitatively associated with decreasing content of the intrinsic defect Nb_{Li}. In terms of this model, a higher v_{tr} in LN-4Zn is caused by a decreased number of Nb-antisites serving as pinning centers for the domain walls.

We now shortly present e-beam domain recording in the heavily-doped crystal LN-7.5Zn. Unfortunately, a high nonuniformity of these samples did not permit us to obtain reproducible curves $l_d(t_{irr})$. The main dissimilarity as compared to CLN and LN-4Zn is that in LN-7.5Zn a much higher implanted charge is required to initiate the domain formation process. Under the same irradiation conditions as used before ($U_0 = 25$ kV, $I = 0.1$ nA) no domains appeared in LN-7.5Zn up to $t_{irr} = 1000$ ms. Recording was achieved through a rise of current to $I = 1$ nA. Using the exposure times in the range of $t_{irr} = 200$–600 ms and irradiation areas of $S = 2 \times 2$, 4×4, and 5×5 μm^2, we succeeded in producing rather long domains of up to 600 μm in length. The implanted charge of $Q =$ 300–500 pC triggering the domain appearance in LN-7.5Zn is by two orders of magnitude higher than in CLN and LN-4Zn. The most probable reason for this is an increased dark conductivity in LN-7.5Zn, which leads to increasing leakage currents during e-beam irradiation [13–16].

3.2 Planar domain gratings recorded in $LiNbO_3$-4 %Zn crystals

The fabrication of domain gratings in LN-4Zn was performed with the aid of the experimental setup identical to one used in [8, 9] (Fig. 4).

A domain grating is fabricated by means of the point-to-point displacement of an e-beam along the *Z*- and *X*- directions with the specified distances L and Λ, respectively, between the points (Fig. 4).

The recording of a grating in LN-4Zn is illustrated by Fig. 5. This grating was recorded using the following experimental conditions: $U_0 = 25$ keV, $I = 0.1$ nA, the local irradiation areas $S = 1$ μm^2, the local irradiation time $t_{irr} = 150$ ms, $L = 15$ μm, and $\Lambda = 8$ μm. In the course of sequential local irradiations along the $+Z$-direction, the domains nucleated in neighboring points separated by the distance L are merging together (Fig. 5a), which leads to formation of a quasi-linear extended domain. The sequential displacements of local irradiations along the *X*-direction produce a domain grating with the spatial period Λ. In the early stage of the process the grating is rather

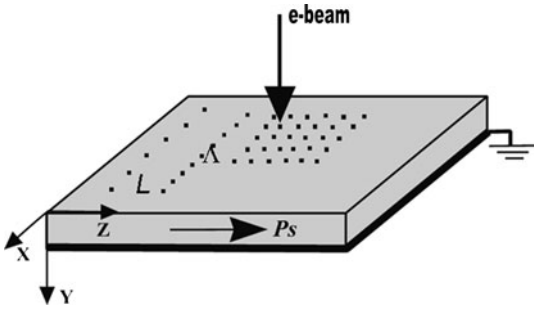

Fig. 4 The scheme of the e-beam recording on the *Y*-surface. *L* and Λ are the distances between the irradiation points along the *Z*- and *X*-axes, respectively

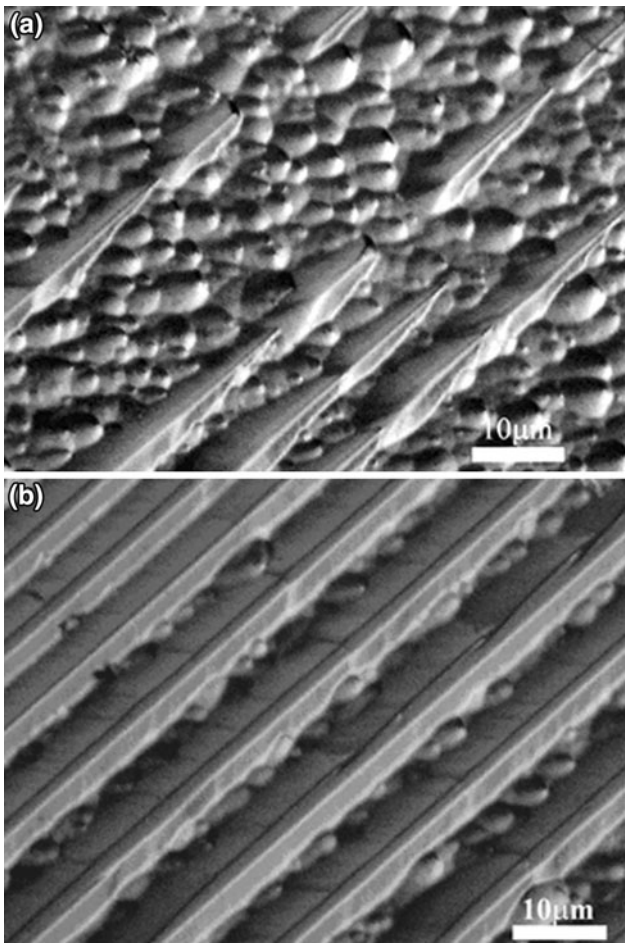

Fig. 5 Recording of a domain grating in $LiNbO_3$-4 %Zn. **a** the initial stage: domains nucleated in neighboring points tend to merge; **b** the final stage: the number of rows of irradiated points aligned parallel to the *X*-axis exceeds 10, the grating becomes regular. The exposure conditions were $U_0 = 25$ keV, $I = 0.1$ nA, $S_{irr} = 1$ μm^2, in all points $t_{irr} = 200$ ms; $L = 20$ μm, $\Lambda = 8$ μm

disturbed (Fig. 5a). It gradually improves with increasing number of the rows of irradiated points parallel to the *X*-axis (Fig. 5 b).

In the following we discuss the fields responsible for the formation of a domain grating. A point-to-point electron charging of the surface of an insulator generates a set of point space charges Q_{sc}. Owing to an extremely low conductivity of $LiNbO_3$ $\sigma = 10^{-14}$–10^{-16} Ohm^{-1} m^{-1} [1], the dielectric relaxation time $\tau_M = \varepsilon\varepsilon_0/\sigma \geq 10^4$–$10^6$ s. As the total recording time of a grating with linear dimensions, say, 500 × 500 μm^2 is of about $t_{rec} \approx 250$ s, consequently $\tau_M >> t_{rec}$ even taking into account a radiation-induced increase of the conductivity. It is reasonable to assume that in the course of recording a grating, the charges Q_{sc} persist in all points without decaying, so that the grating is produced by the total field of point charges $\vec{E} = \sum_{i=1}^{n} \vec{E}_i$, where E_i is the space-charge field in every irradiation point, and n is the number of points.

To verify this statement, we investigated domain arrays generated by spaced single rows of point charges Q_{sc} aligned parallel to the *X*-axis. A single row of Q_{sc} was produced by a point-to-point e-beam displacement along the *X*-axis with a fixed distance Λ between the points. As a result, the domains nucleating at every point of the row are growing along the $+Z$ direction forming a comb-shaped grating with the period Λ and a length l_d. In the center part of the "comb", l_d is slightly larger than along the edges. Two domain gratings were fabricated by means of recording two spaced rows of Q_{sc} with $\Lambda = 10$ and 30 μm; the number of irradiation points in each row was $n = 20$. Figure 6 presents the dependencies of the averaged domain lengths l_d in these gratings on the local irradiation time t_{irr} One may see a noticeable increase of l_d with the decrease of Λ.

The strength of the field E_z at a distance l_d from a row of point charges Q_{sc} aligned parallel to the *X*-axis can be presented by a simplified expression:

$$E = \sum E_i = \frac{Q_{sc} l_d}{2\pi\varepsilon_0\sqrt{\varepsilon_z\varepsilon_x}} \sum_{i=0}^{n} \frac{1}{\left[l_d^2 + (n_i\Lambda)^2\right]^{3/2}} \quad (5)$$

where n and Λ are, respectively, the number of points and the distance between them. We evaluated the fields E given by two charged rows with $\Lambda = 10$ and 30 μm by substituting into Eq. (5) the averaged values $l_d = 300$ and 90 μm achieved in these gratings at $t_{irr} = 300$ ms (Fig. 6). This evaluation gives $E = 5.4\ 10^6$ and $2\ 10^6$ V/m for $\Lambda = 10$ and 30 μm, respectively. The plot $l_d(t_{irr})$ for $\Lambda = 30$ μm (Fig. 6) is very close to that obtained for the individual domains (Fig. 2). A good agreement of the simplified calculations of the fields generated by single rows of point charges with the experimental data (Fig. 6) suggests the addition of space-charge fields. In a real situation (Fig. 5), a domain grating is produced by a set of charged rows spaced at an interval L along the *Z*-axis. The expression for

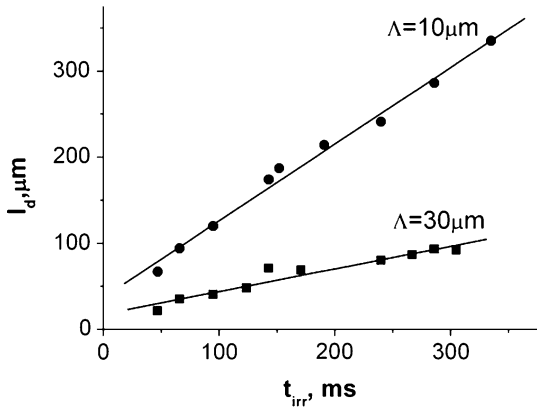

Fig. 6 The exposure dependencies of the averaged l_d in two domain gratings generated by two single rows of the irradiation points. The rows were aligned parallel to the *X*-axis; the distances between the irradiation points were 10 and 30 μm, in any point $t_{irr} = 300$ ms

the field $\vec{E} = \sum_{i=1}^{n} \vec{E}_i$ becomes very cumbersome. Due to the additive effect of "point" fields, the local irradiation times $t_{irr} \approx 100$–150 ms required for fabrication of a grating 500×500 μm^2 in size, are appreciably lower than t_{irr} required for recording individual domains of the same length (Fig. 2). Or, in other words, at equal L and t_{irr}, the smaller the period, the more extended the grating. Interestingly, the length of the domains freely growing from the last row of charges reaches sometimes $l_d \sim 500$–600 μm, which is due to the fact that the total field approaches its maximum towards the last row.

4 Conclusions

We investigated the formation of "individual" (single) domains under electron beam irradiation of the nonpolar *Y*-surfaces of pure and Zn-doped $LiNbO_3$ crystals. Under a local irradiation of the *Y*-surface, a domain arises at the irradiation point due to the formation of a space-charge field E_{sc} induced by the electron beam. The domain is growing frontally along the $+Z$ direction within the surface layer of several microns in thickness. The domain length l_d grows with the irradiation time t_{irr} with no tend to saturation, whereas the domain width is practically independent of t_{irr}. The obtained dependencies $l_d(t_{irr})$ are discussed in the framework of the current approach to the e-beam charging of insulators. It is suggested that a salient point in the plots $l_d(t_{irr})$ at certain irradiation time corresponds to the occurrence of the dynamic charge equilibrium. Consequently, the field reaches a quasi-steady state $E_{sc} = \text{const}$ resulting in a constant velocity of the frontal domain growth, $v_{tr} = \text{const}$, which accounts for the linearity of $l_d(t_{irr})$. We thus conclude that frontal domain growth occurring in a thin surface layer, proceeds by the mechanism of viscous friction. The evaluation of the fields based both on the $l_d(t_{irr})$ curves and the irradiation doses permit us to assume that the frontal domain growth happens up to the fields $E < E_c$ The velocity of the domain growth in $LiNbO_3$-Zn exceeds v_{tr} in CLN, which in terms of the model of $LiNbO_3$ defect structure may be attributed to a decreased number of Nb_{Li} defects serving as pinning centers for the domain motion.

In $LiNbO_3$-4 %Zn crystals planar domain gratings with a period of about 8 μm were fabricated by means of a point-to-point displacement of the e-beam along the *Z*- and *X*-directions with specified distances between the irradiation points. It is shown that the grating is recorded in a total field of point charges $\vec{E} = \sum_{i=1}^{n} \vec{E}_i$, where E_i is the space-charge field in an irradiation point and n is the number of points. This provides a possibility of producing extended domain arrays with the use of local irradiation times significantly shorter than those required for recording individual domains of the same length.

Acknowledgments The authors thank E. I. Rau for the useful consultations and E. Soergel for her help. This work was partially supported by the Russian Foundation for Basic Researches (Project No. 12-02-00596-a) and the Ministry of Education and Science of Russian Federation (State Contract no. 16.513.11.3142).

References

1. T. Volk, M. Wöhlecke, *Lithium Niobate: Defects, Photorefraction and Ferroelectric Switching* (Springer, Berlin, 2008)
2. J. Webjoern, F. Laurell, G. Arvidsson, J. Lightwave Technol. **7**, 1597 (1989)
3. A.C.G. Nutt, V. Gopalan, M.C. Gupta, Appl. Phys. Lett. **60**, 2828 (1992)
4. C. Restoin, C. Darraud-Taupiac, J.L. Decossas, J.C. Vareille, J. Hauden, A. Martinez, J. Appl. Phys. **88**, 6665 (2000)
5. J. He, S.H. Tang, Y.Q. Qin, P. Dong, H.Z. Zhang, C.H. Kang, W.X. Sun, Z.X. Shen, J. Appl. Phys. **93**, 9943 (2003)
6. A.C. Busacca, C.L. Sones, R.W. Eason, S. Mailis, Ferrolectrics **296**, 91 (2003)
7. Y. Glickman, E. Winebrand, A. Arie, G. Rosenman, Appl. Phys. Lett. **88**, 011103 (2006)
8. L.S. Kokhanchik, D.V. Punegov, Proc. SPIE **7025**, 70250J (2008)
9. L.S. Kokhanchik, M.V. Borodin, S.M. Shandarov, N.I. Burimov, V.V. Shcherbina, T.R. Volk, Phys. Sol. State **52**, 1722 (2010)
10. W.M. Young, R.S. Feigelson, M.M. Fejer, M.J.F. Digonnet, H.J. Shaw, Opt. Lett. **16**, 995 (1991)
11. O. Norio, I. Takashi, J. Appl. Phys. **46**, 1063 (1975)
12. V.A. Dyakov, I.V. Yaminsky, DYu. Gavrilko, N.F. Evlanova, I.I. Naumova, V. Ya.Shur, Ferroelectrics **341**, 131 (2006)
13. Z.G. Song, C.K. Ong, H. Gong, J. Appl. Phys. **79**, 7123 (1996)
14. J. Cazaux, J. Appl. Phys. **85**, 1137 (1999)
15. E.I. Rau, E.N. Evstafeva, M.V. Andrianov, Phys. Sol. State **50**, 621 (2008)
16. S. Fakhfakh, O. Jbara, S. Rondot, A. Hadjadj, J.M. Patat, Z. Fakhfakh, J. Appl. Phys. **108**, 093705 (2010)
17. A.E. Grun, Z. Naturforsch, A **12**, 89 (1957)
18. D.B. Wittry, D.F. Kyser, J. Appl. Phys. **38**, 375 (1967)
19. J. Goldstein, H. Yakowitz (eds), *Practical Scanning Electron Microscopy,* vol. 18 (Plenum, New York, 1975)
20. E. Fatuzzo, W.J. Merz, *Ferroelectricity* (North-Holland, Amsterdam, 1966)
21. A. K. Tagantzev, L. E. Cross, J. Fousek, *Domains in Ferroic Crystals and Thin Films*, (Springer Science, 2010)
22. D.B. Li, D.R. Strachan, J.H. Ferris, D.A. Bonnell, J. Mater. Res. **21**, 935 (2006)
23. L.-H. Peng, Y.-C. Zhang, Y.-C. Lin, Appl. Phys. Lett. **78**, 4 (2001)
24. Y.-L. Chen, W.-G. Yan, J. Guo, Sh.-L. Chen, G.-G. Zhang, Z.-R. Xia, Appl. Phys. Lett. **87**, 212904 (2005)
25. S.O. Fregatov, A.B. Sherman, Tech. Phys. Lett. **23**, 438 (1997)
26. S.O. Fregatov, A.B. Sherman, Phys. Solid State **41**, 457 (1999)
27. V.G. Zalesskii, S.O. Fregatov, A.B. Sherman, Phys. Solid State **43**(9), 1739 (2001)
28. G. Rosenman, P. Urenski, A. Agronin, Y. Rosenwaks, M. Molotskii, Appl. Phys. Lett. **82**, 103 (2003)
29. M. Molotskii, J. Appl. Phys. **93**, 6234 (2003)
30. K. Nakamura, J. Kurz, K. Paramerswaran, M.M. Fejer, J. Appl. Phys. **91**, 4528 (2002)